Journal of Alloys and Compounds 509 (2011) 5545–5550

Contents lists available at ScienceDirect

Journal of Alloys and Compounds

journal homepage: www.elsevier.com/locate/jallcom

# Changes in the microstructure and hydrogen storage properties of Ti–Cr–V alloys by ball milling and heat treatment

Sung-Wook Cho*, Jeong-Hyun Yoo, Han-Kwon Chang, Won-Baek Kim, Dae-Sup Kil, Jong-Gwan Ahn

*Industrial Materials Research Department, Korea Institute of Geoscience & Mineral Resources, 92 Gwahang-no, Yuseong-gu, Daejeon 305-350, Republic of Korea*

ARTICLE INFO

*Article history:*
Received 22 October 2010
Received in revised form 1 February 2011
Accepted 2 February 2011
Available online 17 February 2011

*Keywords:*
Hydrogen absorbing materials
Ti–Cr–V alloy
X-ray diffraction
Mechanical milling
Microstructure

ABSTRACT

Changes in the microstructure and hydrogen storage properties of Ti–Cr–V alloys were investigated after a combination of ball milling and heat treatment. Two different sets of balls and vials made of tungsten carbide (WC) and stainless steel (STS) were used for milling the samples. Ball milling using WC balls and vials induced WC contamination, and it caused compositional changes in the matrix during heat treatment. When STS balls and vials were used, meanwhile, no peak of the second phase caused by contamination was found in the X-ray diffraction (XRD) data. In the case of the sample that completed only the milling process, the crystallite size calculated from the XRD data, 20–30 nm, agreed well with the grain size obtained from transmission electron microscopy (TEM). On the other hand, for the sample that was heat treated after milling, the strain decreased from 0.74% to 0.18%, the crystallite size increased to 70–80 nm, and the grain size grew up to the level of hundreds of nanometers. The changes in microstructure induced by the ball milling and heat treatment influenced the hydrogen storage properties, such as plateau pressure, hysteresis, and phase transformation with hydrogen absorption. Thus, the relationship between the microstructure and hydrogen storage properties can be explained.



## 1. Introduction

Modern industrial society developed based on coal and oil energy, but their use entails unstable supply-demand issues and air pollution problems. Thus, many studies of hydrogen as a clean energy carrier have been conducted in order to replace fossil fuels. However, because hydrogen exists as a gas at room temperature and atmospheric pressure, it is difficult to store and transport, and to solve this problem, many studies of various methods for storing hydrogen are in progress [1,2].

Hydrogen storage alloy with body centered cubic (BCC) structure is considered one of the promising candidates to effectively store hydrogen because it can absorb a large amount of hydrogen per metal atom (H/M) at around normal temperature and pressure [3–7]. In general, BCC alloys containing Ti or V have two plateau pressures that correspond to the formation of the mono-hydride (MH) and di-hydride ($MH_2$). However, the hydrogen (about 1.5 wt%) absorbed during the formation of the mono-hydride is hard to use because it is not desorbed at room temperature due to its low desorption plateau pressure [8–10].

The addition of B, Al, etc. into Ti–Cr–V alloy [11,12] with a BCC structure was investigated for the purpose of reducing the residual hydrogen [13,14], which was not desorbed even at low pressure. The addition of these elements, however, resulted in a severe decrease in the hydrogen storage capacity. In addition, no reduction of the residual hydrogen was observed.

Kabutomori et al. [15] reported that the formation of the di-hydride of the $Ti_{24}Cr_{36}V_{40}$ alloy could be enhanced by reducing the particle size and internal defects with heat treatment. They suggested that the internal defects were reduced by the fine particle size and heat treatment, which limited the formation of the mono-hydride during hydrogenation. However, the explanations for those were insufficient, and it should also be noted that there were limitations on the particle size because they used simple agate to crush the powders.

In this study, using a Ti–Cr–V alloy that exhibited superior hydrogen storage capacity in our previous studies [11,12], changes in the microstructure and hydrogen storage properties were investigated after a combination of ball milling and heat treatment, and the relationship between the microstructure and hydrogen storage properties was discussed.

## 2. Experimental procedure

Button-type alloy ingots weighing about 20 g each were prepared by arc melting Ti, Cr and V granules. The purities of Ti, Cr and V were higher than 99.8%, 99.4% and 99.9%, respectively. The alloy was melted in a cold Cu crucible under ultra high-purity Ar gas. To homogenize the alloy composition, the buttons were turned over and remelted five times.

* Corresponding author. Tel.: +82 42 868 3632; fax: +82 42 868 3415.
*E-mail address:* cho@kigam.re.kr (S.-W. Cho).

0925-8388/$ – see front matter © 2011 Elsevier B.V. All rights reserved.
doi:10.1016/j.jallcom.2011.02.005

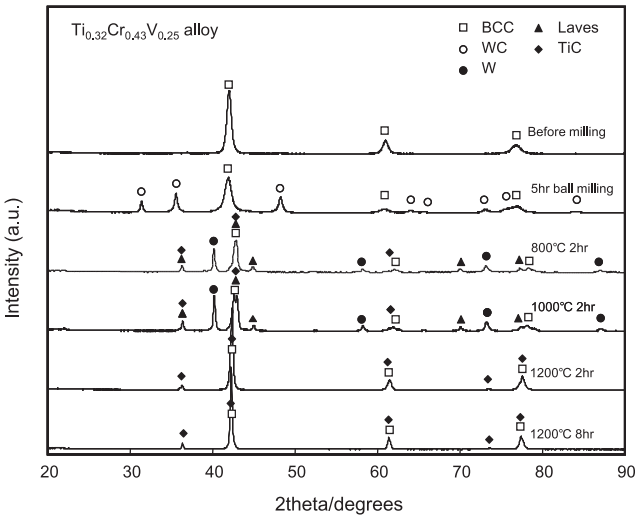


**Fig. 1.** X-ray diffraction patterns of the $Ti_{0.32}Cr_{0.43}V_{0.25}$ alloy obtained after ball milling for 5 h and subsequent heat treatment.

The alloy was milled for 0–20 h using a planetary type ball mill. Powder precrushed to 100–200 μm was used for milling. Two different sets of balls and vials made of tungsten carbide (WC) and stainless steel (STS) were used. The weight ratio of the sample and balls was 1:10. The milled powders were heat treated in a vacuum of $10^{-5}$ Torr.

The crystal structure of the samples was examined with a Rigaku X-ray diffractometer using Cu Kα radiation (λ = 0.154178 nm). Transmission electron microscopy (TEM, JEOL 2100F HR) and energy dispersive X-ray spectroscopy (EDS) were used to examine the microstructure and the chemical composition of the powders. The specimens for TEM observation were prepared using a focused ion beam. Pressure-composition (P-C) isotherms were measured using about 1 g of powder in a Sievert's type apparatus at 293 K.

## 3. Results and discussion

Balls and vials made of WC were used for milling $Ti_{0.32}Cr_{0.43}V_{0.25}$ alloy. To investigate the changes in microstructure, the sample powders were analyzed using powder X-ray diffraction method. The results are shown in Fig. 1. The X-ray diffraction (XRD) peaks became broader after milling for 5 h due to the fine particle size. In addition, the WC phase was observed, obviously caused by contamination during milling. The WC reacted with Ti in the alloy to form TiC and W during subsequent heat treatment. The Laves phase was also found after heat treatment at 800–1000 °C, which will be explained later. While TiC remained as the second phase at all conditions, W was dissolved in the BCC matrix.

Because of the above, the BCC lattice parameter of the sample that was heat treated at 1200 °C for 8 h was decreased to 0.30138(1) nm compared to that of the sample before milling (0.30397(1) nm ($R_{wp}$ = 18.83, $S$ = 2.649)), which were obtained by Rietveld analyses for the X-ray diffraction data using GSAS. Fig. 2 and Table 1 show the results of Rietveld refinement for the sample that was heat treated at 1200 °C for 8 h.

The hydrogen storage capacity of each sample shown in Fig. 1 markedly decreased within the limited measuring range (approx. 5 MPa) due to the contamination, the second phases and the decrease in lattice parameter. P-C isotherms of these samples are left out in this paper.

**Table 1**
The parameters of the sample obtained from Fig. 2 using X-ray Rietveld analysis.

| Specimen | Phase | Space group (no.) | $a$ (nm) | Phase (%) |
|---|---|---|---|---|
| $Ti_{0.32}Cr_{0.43}V_{0.25}$, 1200 °C, 8 h | | | | |
| $R_{wp}$ = 13.35 | BCC | *Im3m* (229) | 0.30138(1) | 88.08 |
| $S$ = 2.075 | TiC | *Fm3m* (225) | 0.4247(1) | 11.92 |

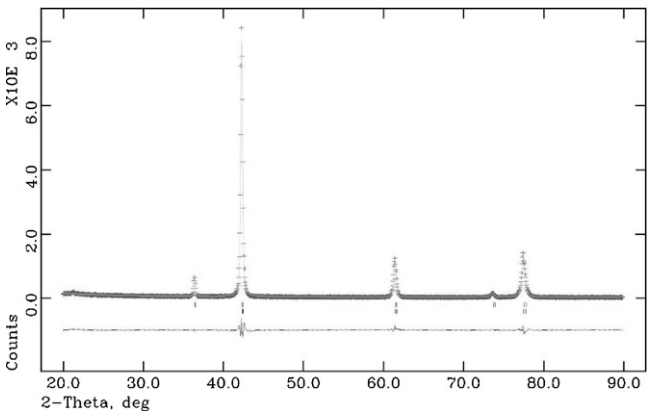


**Fig. 2.** Rietveld analysis of the $Ti_{0.32}Cr_{0.43}V_{0.25}$ alloy obtained after ball milling for 5 h and subsequent heat treatment at 1200 °C for 8 h.

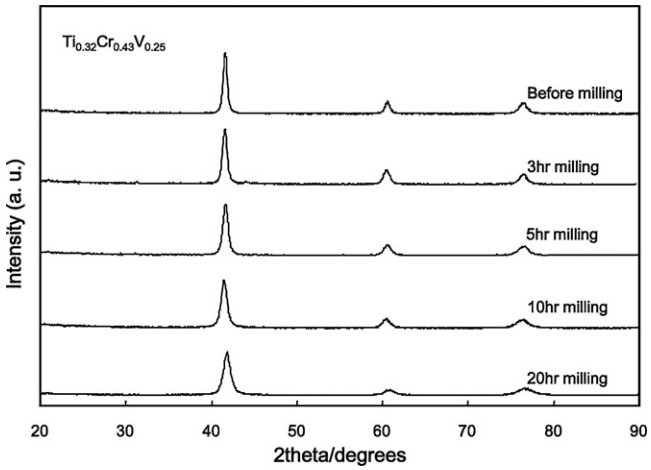


**Fig. 3.** X-ray diffraction patterns of the $Ti_{0.32}Cr_{0.43}V_{0.25}$ alloys obtained after ball milling for 0–20 h.

To prevent the WC contamination, ball milling was conducted using STS balls and vials. Fig. 3 shows the XRD patterns of the samples that were ball milled for 0–20 h. As shown in this figure, no peak of the second phase caused by the contamination appeared. However, for the sample that was milled for 20 h, EDS analysis showed that about 5 wt% of Fe was present, which is shown in Fig. 4.

To find the optimal milling time to minimize Fe contamination and maximize the effects of ball milling, the changes in the crys-

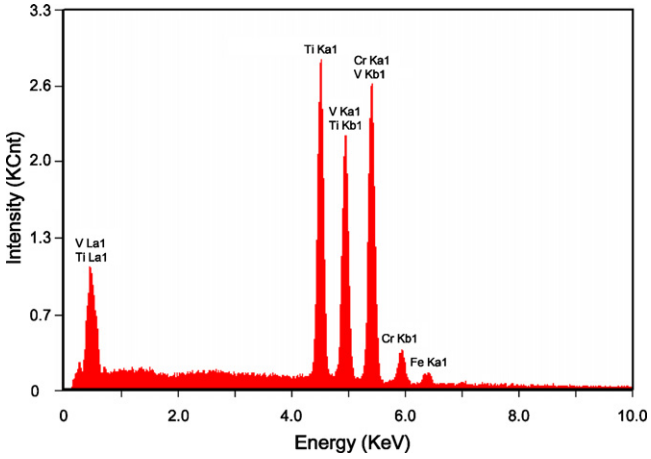


**Fig. 4.** EDS results for the $Ti_{0.32}Cr_{0.43}V_{0.25}$ alloy obtained after ball milling for 20 h.

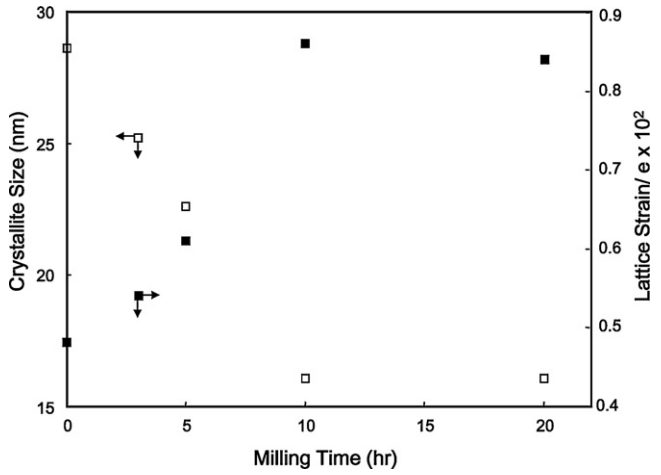


**Fig. 5.** Crystallite size ($D$) and lattice strain ($e$) of the $Ti_{0.32}Cr_{0.43}V_{0.25}$ alloys obtained after ball milling for 0–20 h.

tallite size and strain according to the milling time were examined, and the results are shown in Fig. 5. These values were obtained from the XRD data in Fig. 3 using the Voigt function and the single-line method [16,17]. As shown in Fig. 5, the crystallite size decreased and the strain increased for up to 10 h of milling, and then they did not change much for up to 20 h of ball milling. In other words, 10 h of milling was enough for $Ti_{0.32}Cr_{0.43}V_{0.25}$ alloy.

For mutual comparison, the powder samples before and after milling were each heat treated for 10 min at 1000 °C, and the XRD patterns are shown in Fig. 6. Unfortunately, $Ti_2O$ and a Laves phase were observed in both samples due to heat treatment. $Ti_2O$ is assumed to be an oxide formed by trace oxygen during heat treatment in a vacuum, and the formation of the Laves phase can be explained as follows.

According to the phase diagram of Ti–Cr–V ternary system [18], a small amount of $TiCr_2$ may form because the composition of the $Ti_{0.32}Cr_{0.43}V_{0.25}$ alloy is located at the boundary of a single-phase area (BCC solid solution) and a two-phase coexistence area (BCC + $TiCr_2$) at 1000 °C. Moreover, it is hard to maintain the high temperature phase at room temperature because cooling is slow in the furnace after the powder sample is heat treated. As shown in the ternary phase diagrams in the temperature range of 900–700 °C, more $TiCr_2$ phase can be formed as the composition of $Ti_{0.32}Cr_{0.43}V_{0.25}$ alloy passes the two-phase coexistence area during cooling because it expands more towards lower temperature.

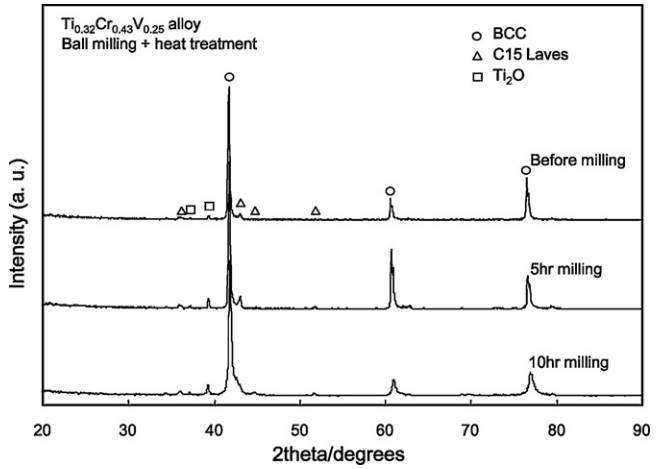


**Fig. 6.** X-ray diffraction patterns of the $Ti_{0.32}Cr_{0.43}V_{0.25}$ alloys obtained after ball milling for 0–10 h and subsequent heat treatment at 1000 °C for 10 min.

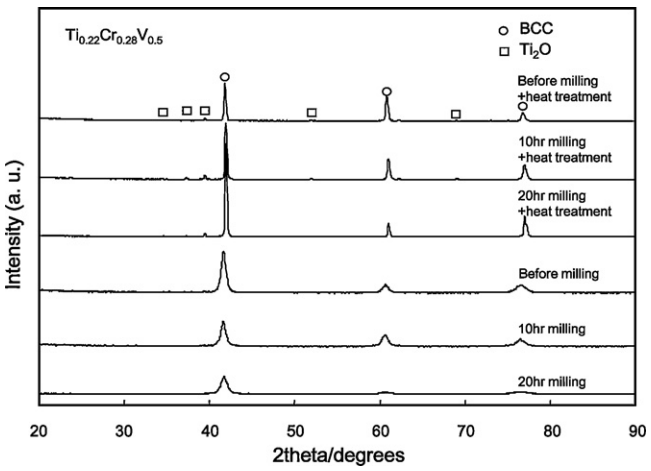


**Fig. 7.** X-ray diffraction patterns of the $Ti_{0.22}Cr_{0.28}V_{0.5}$ alloys obtained after ball milling for 0–20 h and heat treatment at 1000 °C for 10 min.

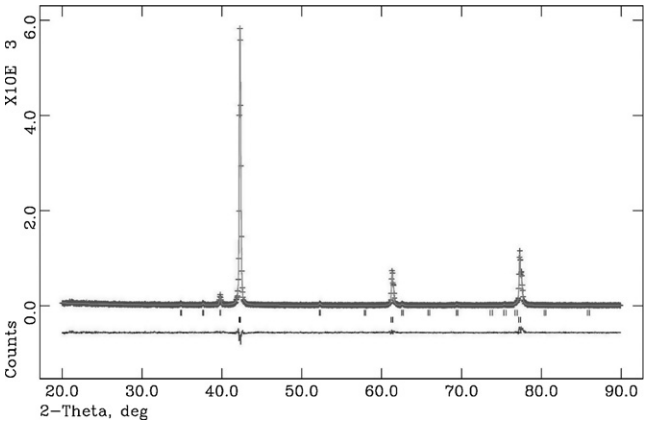


**Fig. 8.** Rietveld analysis of the $Ti_{0.22}Cr_{0.28}V_{0.5}$ alloy obtained after ball milling for 20 h and subsequent heat treatment at 1000 °C for 10 min.

Therefore, an additional experiment was conducted by changing the Ti–Cr–V alloy composition to $Ti_{0.22}Cr_{0.28}V_{0.5}$ to prevent the formation of the $TiCr_2$ phase. This composition was selected by considering the phase diagram of the Ti–Cr–V ternary system according to the temperature within the area that had been reported to have superior hydrogen storage capacity by Cho et al. [19].

The same ball milling and heat treatment were conducted for the $Ti_{0.22}Cr_{0.28}V_{0.5}$ alloy as conducted for $Ti_{0.32}Cr_{0.43}V_{0.25}$ alloy, and the XRD pattern of each step is shown in Fig. 7. There was no peak caused by contamination as in Fig. 3. In addition, the Laves phase was not observed in the sample that completed heat treatment, unlike in the $Ti_{0.32}Cr_{0.43}V_{0.25}$ alloy. This result suggests that the explanation for the cause of Laves phase formation is sufficient. The result of Rietveld refinement for the sample that was heat treated for 10 min at 1000 °C after 20 h of milling is representatively presented in Fig. 8, and the results are summarized in Table 2.

As shown in Table 2, the formation of the Laves phase was suppressed, but $Ti_2O$ was still formed (4.8(2) wt%) with heat treatment. The formation of $Ti_2O$ caused the changes in the Ti

**Table 2**
The parameters of the sample obtained from Fig. 8 using X-ray Rietveld analysis.

| Specimen | Phase | Space group (no.) | $a$ (nm) | $c$ (nm) | Phase (%) |
|---|---|---|---|---|---|
| $Ti_{0.22}Cr_{0.28}V_{0.5}$, 1000 °C, 10 min | | | | | |
| $R_{wp}$ = 18.41 | BCC | *Im3m* (229) | 0.30246(1) | | 95.24(3) |
| $S$ = 1.825 | $Ti_2O$ | *P3m1* (156) | 0.29681(4) | 0.4776(1) | 4.8(2) |

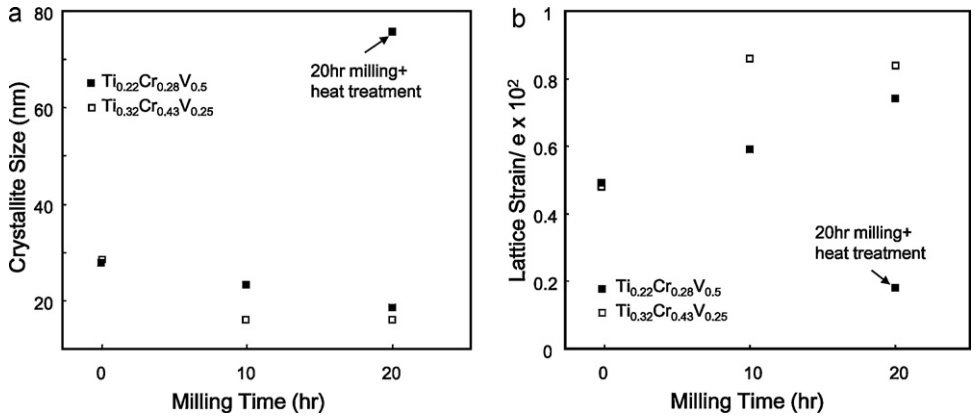


**Fig. 9.** Crystallite size ($D$) and lattice strain ($e$) of the Ti–Cr–V alloys obtained after ball milling for 0–20 h and subsequent heat treatment: (a) crystallite size and (b) lattice strain.

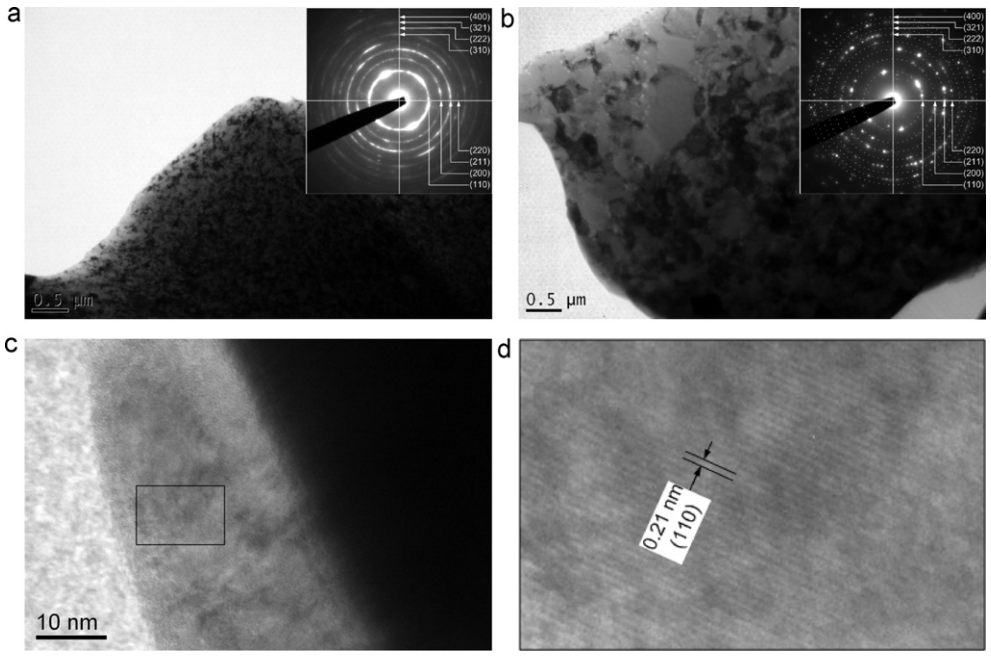


**Fig. 10.** TEM images of the $Ti_{0.22}Cr_{0.28}V_{0.50}$ alloy obtained after ball milling and heat treatment. (a) BF image after ball milling for 20 h, (b) BF image after subsequent heat treatment at 1000 °C for 10 min, (c) BF image of powder magnified to 400,000 times and (d) expanded figure of the marked part in (c).

content of the matrix and its lattice parameter. Namely, by calculating the compositional change of the matrix when 4.8(2) wt% of $Ti_2O$ forms, the alloy composition changes to $Ti_{0.19}Cr_{0.29}V_{0.52}$ due to a reduction of the Ti content, and the lattice parameter thus decreases from 0.30351(1) nm ($R_{wp}$ = 16.40, $S$ = 1.946) before milling to 0.30246(1) nm after milling and heat treatment.

Changes in the crystallite size and strain of the $Ti_{0.22}Cr_{0.28}V_{0.5}$ alloy with milling and heat treatment are shown in Fig. 9. The crystallite size and strain of the sample milled for 20 h showed values similar to those of the $Ti_{0.32}Cr_{0.43}V_{0.25}$ alloy milled for 10 h. The crystallite size and strain of the $Ti_{0.22}Cr_{0.28}V_{0.5}$ alloy changed from 28.2 nm and 0.49 % to 18.5 nm and 0.74%, respectively, after 20 h of milling, and then changed to 75.7 nm and 0.18% due to heat treatment. These data imply that the sample with the reduced internal defects was produced by heat treatment.

To confirm the change in microstructure directly, TEM observation was conducted on the sample after 20 h of milling and on the sample heat treated after milling. The results are shown in Fig. 10. The grain size of the milled sample was at the level of several tens of nanometers, as shown in the TEM image, Fig. 10a, which matched the crystallite size calculated from the XRD data. In addition, it was confirmed that the crystal structure was BCC by calculating ring distance of the SAD pattern shown in the inset of Fig. 10a. The clear ring patterns implied that the crystallite size was minute. The terms of crystallite and grain create some confusion, so it is needed to clarify their meanings. Crystallite is a more general term and may mean a domain in the cases of a cold-worked and partially annealed metal or a grain in the cases of a perfectly well-annealed metal and nano crystalline material. In a nano crystalline material the grain size is so small (~10–100 nm) that it will not be possible to have a substructure. Therefore, in this case, crystallite and grain all mean the same thing [20].

On the other hand, the grain size of the sample that was heat treated was at the level of hundreds of nanometers, as shown in the TEM image in Fig. 10b. It showed a large difference from the crystallite size calculated from XRD data, which implies that

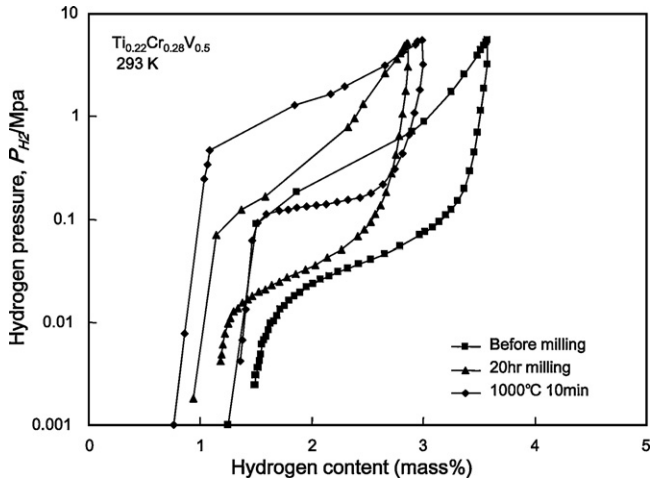


**Fig. 11.** P-C isotherm of the $Ti_{0.22}Cr_{0.28}V_{0.5}$ alloy obtained after ball milling and heat treatment at 1000 °C for 10 min.

the grains, which grew during heat treatment, formed a substructure consisting of individual crystallites. In addition, the SAD pattern shown in the inset in Fig. 10b showed a dotted pattern, even though the same size of diffraction aperture was used. Each dot was located on a virtual circle that represents a BCC structure, as in Fig. 10a, which means that the crystallite size was large compared to that of the sample before heat treatment, and the crystal structure had the same BCC structure as before heat treatment.

Fig. 10c shows the bright field image of the powder obtained after heat treatment, which was magnified to 400,000×. The plane spacing calculated using Fig. 10d, which is the expanded view of the marked part of Fig. 10c, was 0.21 nm. This value agreed well with that of the (1 1 0) plane, 0.208 nm, which was calculated from the lattice parameter (0.30246(1) nm) obtained from Rietveld refinement, as shown in Table 2.

P-C isotherms of the samples before ball milling, those milled for 20 h, and those heat treated after milling are compared in Fig. 11. The hydrogen storage capacity of the milled sample decreased, and the slope of the plateau became steep, which is assumed to be caused by an increase in the strain due to milling [21,22]. For the sample heat treated after milling, the hydrogen storage capacity decreased within the limited measuring range as the plateau pressure increased significantly. This result can be understood by the reduction of the lattice parameter, as shown in Table 2. Namely, because hydrogen absorbed in the alloy occupies the interstitial site and its size decreases with the reduction of the lattice parameter, the plateau pressure increases with the reduction of the lattice parameter [19,23]. In addition, an increase of the hysteresis was also observed, which was in good agreement with the previous report [14] that a decrease of the strain and an increase of the crystallite size increase the hysteresis.

Moreover, the plateau region of the absorption curve shifted to the left considerably compared to that of the sample before milling. If this shift is caused by insufficient activation, then the width of the plateau region must decrease by this ratio. However, the width of the plateau region was similar to that of the sample before milling. Therefore, it is assumed that some of the sample exhibited the same phenomenon which Kabutomori et al. reported to be the direct phase transformation from α to γ.

This phenomenon can be understood as follows. The internal defects of the sample heat treated after milling were removed as mentioned before. Various internal defects as vacancies and dislocations can act as a short path for hydrogen, which allows an early accommodation of hydrogen into the alloy. Therefore, the removal or reduction of easy path makes the diffusion of hydrogen and the formation of hydrogen-rich phase more difficult. This makes the hydrogenation of the sample heat treated after milling become less favorable both energetically and kinetically at lower hydrogen pressure, which resulted in the shift of the P-C isotherm towards left side as observed in Fig. 11.

## 4. Conclusions

The results are summarized as follows. WC contaminated by ball milling reacted with Ti in the alloy to form TiC and W during heat treatment. TiC was precipitated as a second phase and W was dissolved in the matrix by the heat treatment at 1200 °C for 2 h, forming a BCC Ti–Cr–V–W solid solution. When STS balls and vials were used, meanwhile, the peak of the second phase caused by contamination was not found in the XRD data. In the case of the $Ti_{0.32}Cr_{0.43}V_{0.25}$ alloy, the Laves phase and a small amount of $Ti_2O$ were formed by heat treatment after milling. The Laves phase was formed in a furnace cooling process after heat treatment of the powder sample. Therefore, the formation of the Laves phase could be suppressed after heat treatment by changing the alloy composition to $Ti_{0.22}Cr_{0.28}V_{0.5}$ based on the phase diagram of the Ti–Cr–V ternary system. However, a small amount of $Ti_2O$ was still formed, which caused changes in Ti content of the matrix and its lattice parameter. In the case of the sample that was only milled, the crystallite size calculated from the XRD data, 20–30 nm, agreed well with the grain size obtained from TEM observation. On the other hand, in the case of the sample that was heat treated after milling, the strain decreased from 0.74% to 0.18%, the crystallite size increased to 70–80 nm, and the grain size grew to the level of hundreds of nanometers. The plateau pressure and hysteresis of the hydrogen storage properties increased in the sample that was heat treated after ball milling. In addition, the plateau region of the absorption curve considerably shifted to the left compared to that of the sample before milling. These changes in hydrogen storage properties could be explained by changes in microstructure, resulting from a combination of ball milling and heat treatment.

## Acknowledgement

This work was carried out as part of the 21st Frontier R&D Program for Hydrogen Energy, supported by the Ministry of Education, Science and Technology of Korea.

## References

[1] A. Zuttel, Mater. Today 6 (2003) 24–33.
[2] D.G. Ivey, R.I. Chittim, K.J. Chittim, D.O. Northwood, J. Mater. Energy Syst. 3 (1981) 3–19.
[3] J.J. Reilly, R.H. Wiswall Jr., Inorg. Chem. 9 (1970) 1678–1682.
[4] S. Ono, K. Nomura, Y. Ikeda, J. Less-Common Met. 72 (1980) 159–165.
[5] G.G. Libowitz, A.J. Maeland, Mater. Sci. Forum 31 (1988) 177–196.
[6] T. Kabutomori, H. Takeda, Y. Wakisaka, K. Ohnishi, J. Alloys Compd. 231 (1995) 528–532.
[7] E. Akiba, H. Iba, Intermetallics 6 (1998) 461–470.
[8] Y. Nakamura, E. Akiba, J. Alloys Compd. 311 (2000) 317–321.
[9] Y. Nakamura, E. Akiba, J. Alloys Compd. 345 (2002) 175–182.
[10] S.W. Cho, H. Enoki, T. Kabutomori, C.N. Park, E. Akiba, J. Alloys Compd. 319 (2001) 196–203.
[11] S.W. Cho, C.N. Park, J.H. Yoo, J. Choi, J.S. Park, C.Y. Suh, G. Shim, J. Alloys Compd. 403 (2005) 262–266.
[12] S.W. Cho, G. Shim, G.S. Choi, C.N. Park, J.H. Yoo, J. Choi, J. Alloys Compd. 430 (2007) 136–141.
[13] S.W. Cho, J.H. Yoo, G. Shim, C.N. Park, J. Choi, Int. J. Hydrogen Energy 33 (2008) 1700–1705.
[14] J.H. Yoo, G. Shim, J.S. Yoon, S.W. Cho, Int. J. Hydrogen Energy 34 (2009) 1463–1467.

[15] T. Kabutomori, K. Kubo, H. Arashima, H. Itoh, T. Suda, S. Ohnuki, K. Onisi, Improving a Rechargeable Hydrogen Storage Capacity of BCC Alloy by Eliminating Internal Defects, TMS 2006 135th Annual Meeting.
[16] Th.H. de Keijser, J.I. Langford, E.J. Mittemeijer, A.B.P. Vogels, J. Appl. Crystallogr 15 (1982) 308–314.
[17] B.K. Singh, G. Shim, S.W. Cho, Int. J. Hydrogen Energy 32 (2007) 4961–4965.
[18] J.Y. Lee, J.H. Kim, S.I. Park, H.M. Lee, J. Alloys Compd. 291 (1999) 229–238.
[19] S.W. Cho, C.S. Han, C.N. Park, E. Akiba, J. Alloys Compd. 288 (1999) 294–298.
[20] C. Suryanarayana, M. Grant Norton, X-ray Diffraction. A Practical Approach, Plenum Press, New York, 1998.
[21] G. Liang, J. Huot, R. Schulz, J. Alloys Compd. 320 (2001) 133–139.
[22] L. Zaluski, A. Zaluska, P. Tessier, J.O. Strom-Olsen, R. Schulz, J. Alloys Compd. 227 (1995) 53–57.
[23] J.H. Yoo, G. Shim, S.W. Cho, C.N. Park, Int. J. Hydrogen Energy 32 (2007) 2977–2981.